Cationic exchange in nanosized $ZnFe_2O_4$ spinel revealed by experimental and simulated near-edge absorption structure

S. J. Stewart,[1,*] S. J. A. Figueroa,[1,2] J. M. Ramallo López,[1,2] S. G. Marchetti,[3] J. F. Bengoa,[3] R. J. Prado,[4] and F. G. Requejo[1,2]

[1]*IFLP-CONICET and Departamento de Física, Facultad Ciencias Exactas, C.C. 67, Universidad Nacional de La Plata, 1900 La Plata, Argentina*

[2]*INIFTA (Facultad Ciencias Exactas, UNLP and CONICET), C.C. 16 sucursal 4-1900 La Plata, Argentina*

[3]*Departamento de Química, Facultad Ciencias Exactas, Universidad Nacional de La Plata, CONICET, CINDECA, CICPBA, 47 No 257, 1900 La Plata, Argentina*

[4]*Departamento de Física, ICET, UFMT, Av. Fernando Corrêa s/n, CEP 78060-900, Cuiabá-MT, Brazil*

(Received 13 September 2006; revised manuscript received 17 November 2006; published 13 February 2007)

The nonequilibrium cation site occupancy in nanosized zinc ferrites (~6–13 nm) with different degree of inversion (~0.2 to 0.4) was investigated using Fe and Zn *K*-edge x-ray absorption near edge spectroscopy (XANES) and extended x-ray absorption fine structure, and magnetic measurements. The very good agreement between experimental and *ab initio* calculations on the Zn *K*-edge XANES region clearly shows the large $Zn^{2+}(A) \rightarrow Zn^{2+}[B]$ transference that takes place in addition to the well-identified $Fe^{3+}[B] \rightarrow Fe^{3+}(A)$ one, without altering the long-range structural order. XANES spectra features as a function of the spinel inversion were shown to depend on the configuration of the ligand shells surrounding the absorbing atom. This XANES approach provides a direct way to sense cationic inversion in these Zn-containing spinel ferrites. We also demonstrated that a mechanical crystallization takes place on nanocrystalline spinel that causes an increase of both grain and magnetic sizes and, simultaneously, generates a significant augment of the inversion.

DOI: 10.1103/PhysRevB.75.073408 PACS number(s): 61.10.Ht, 81.20.Wk, 61.82.Rx, 75.50.Tt

Several works have demonstrated that when normal spinel ferrite $ZnFe_2O_4$ becomes nanosized it displays a nonequilibrium cation distribution among their tetrahedral (A) and octahedral (B) sites that alters its long-range magnetic ordering and drastically enhances its magnetic response.[1–5] Iron (III) occupancy of both A and B sites in nanocrystalline $ZnFe_2O_4$ has been extensively proved by Mössbauer spectroscopy,[1,2,6–8] nuclear magnetic resonance,[5] neutron diffraction,[3] x-ray absorption,[9–12] and indirectly throughout magnetic measurements.[2–4,13,14] To a much lesser extent, extended x-ray absorption fine structure (EXAFS) studies at Zn *K* edge suggest that Zn ions are transferred from its equilibrium position (sites A) to B sites when the particle size decreases,[9–11] but there is still some lack of clarity concerning Zn nonequilibrium positions and its effects. Some results indicate that Zn nonequilibrium location produces an overpopulation of B sites by both Zn and Fe ions,[10] while other claim that it distorts the spinel structure and brings about an amorphous state.[9] Thus, more studies are needed concerning the less-explored Zn local geometry to completely understand the origin of the nonequilibrium cation distribution in nanosized $ZnFe_2O_4$.

X-ray absorption near edge spectroscopy (XANES) reflects the excitation process of a core electron to bound and quasibound states near to the Fermi level. Even though its intensity is around one order of magnitude larger than that of the EXAFS region and involves a reduced photon energy range (~50 eV), it is dominated by multiple scattering interactions that make the interpretation of XANES spectra substantially more complicated. However, recently improved simulation tools based in *ab initio* XANES calculations such as code FEFF8.2 (Ref. 15) can be employed to better elucidate the XANES features and get some insight into the compound electronic structure.

Here we study the nonequilibrium cation site occupancy in nanosized $ZnFe_2O_4$ and how it affects the XANES spectra at both Fe and Zn *K* edges. Throughout the very good agreement between experimental and theoretical results on the Zn *K*-edge region we show the potentialities of this technique to straightforwardly sense the $Zn^{2+}(A) \rightarrow Zn^{2+}[B]$ transference, in addition to the well-determined $Fe^{3+}[B] \rightarrow Fe^{3+}(A)$ one, that confer peculiar magnetic properties to nanosized $ZnFe_2O_4$. We also show that by milling nanocrystalline $ZnFe_2O_4$ a considerable cation exchange occurs that increases the degree of inversion as the grain and/or particle sizes increase without altering the long-range structure.

$ZnFe_2O_4$ nanoferrite (sample 2ZF) was prepared by precipitating aqueous mixtures of zinc (II) and iron (III) nitrates in a ratio Zn:Fe 1:2 with aqueous ammonia. The suspension was hydrothermally processed in a Teflon-lined autoclave at 250 °C. The product was filtered, washed with distilled water, and dried. Samples 2ZF4h and 2ZF10h were obtained by high-energy ball milling nanocrystalline 2ZF for t_m=4 and 10 h, respectively, in a horizontal miller (Retsch) with a stainless steel vial, and one stainless steel ball (mass to powder ratio was 10:1). Bulk $ZnFe_2O_4$ was prepared by a conventional solid sate reaction. Transmission electronic microscopy was performed in a JEOL JEM-200FX microscope operating at 200 keV. Magnetic measurements were carried out using both commercial superconducting quantum interference device magnetometer and AC susceptometer. ^{57}Fe Mössbauer spectra in the 4.2 to 300 K range of temperature were taken in transmission geometry. EXAFS and XANES spectra of the Fe *K* edge (7112 eV) and Zn *K* edge (9659 eV) were recorded at room temperature in transmission mode using a Si(111) monochromator with a slit aperture of 0.3 mm at the XAS beamline of the LNLS (Laboratório Nacional de Luz Síncrotron) in Campinas, Brazil.

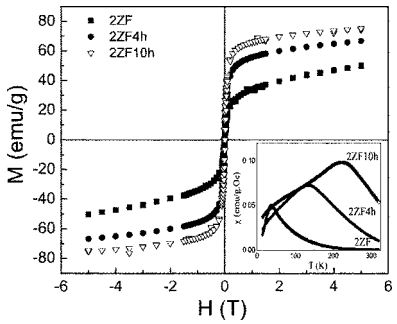

FIG. 1. Magnetization *versus* applied magnetic field (*M-H*) loops taken at 5 K under a maximum field of 5 T for 2ZF, 2ZF4h, and 2ZF10h nanosized zinc ferrites. Inset: thermal dependence of the in-phase ac susceptibility.

Previously,[12] x-ray diffraction studies showed that all of the samples are of single phase $ZnFe_2O_4$ cubic spinel. No amorphous components were detected. In addition, we have observed that milling causes a progressive increment of the average grain size from 6 to 13 nm.[12] Dark field TEM micrographs showed particles in the 4–20 nm range, with average sizes of 6 nm and 8 nm for 2ZF and 2ZF10h, respectively. Atomic absorption showed that the initial Zn:Fe ratio of $\approx 1:2$ was unaltered by milling.

Mössbauer spectra recorded at 4.2 K showed that Fe^{3+} ions occupy both A and B magnetic sublattices.[12] Further, we observed that the relative area ratio site (A): site [B] doubles from 2ZF to 2ZF10h, indicating a milling-induced transference of iron ions from B to A sites. The thermal evolution of the Mössbauer spectra (not shown) associated with susceptibility measurements (Fig. 1) provided evidence for a superparamagnetic relaxation of particle moments. The blocking temperature, T_B, taken as the maximum of the in-phase ac susceptibility, χ', is 38, 135, and 220 K for 2ZF, 2ZF4h, and 2ZF10h, respectively (Fig. 1). The progressive increment of T_B reflects the magnetic size growth with the milling. The *S* shapes displayed by the *M-H* curves (Fig. 1) evidence magnetic states with spontaneous magnetization. Further, the magnetic response rather increases by increasing the milling time as seen by the increment of the saturation magnetization M_S (at $T=5$ K, $M_S=35$, 57, and 68 emu/g for 2ZF, 2ZF4h, and 2ZF10h, respectively). There is also an increment of the magnetic hardness with the grain size (the coercive fields are

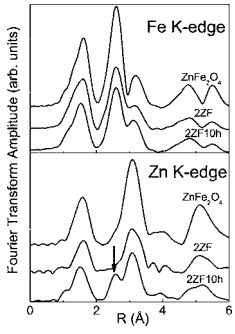

FIG. 2. Fourier transforms of the EXAFS spectra Fe and Zn *K* edges of bulk $ZnFe_2O_4$ and nanosized ferrites 2ZF and 2ZF10h. Arrow indicates the new coordination sphere because large Zn population at *B* sites.

TABLE I. EXAFS Fe *K*-edge fitted parameters. *N* is the coordination number, *R* the distance from central atom, σ^2 the Debye-Waller factor, E_0 the energy shift, and *c* is the degree of inversion determined according to the Fe *K*-edge EXAFS fitted data.

Sample	Shell	*N*	*R* (Å)	σ^2(Å^2)$\times 10^{-2}$	E_0	*c* (%)
2ZF	O	5.5±0.9	1.96±0.03	0.7±0.2	−5±2	22
2ZF10h	O	5.8±0.9	1.97±0.03	0.8±0.2	−5±2	38

87 and 198 Oe for 2ZF and 2ZF10h, respectively). These magnetic and Mössbauer results are compatible with a ferrimagnetic state of the nanoferrites.

The $\chi(k)$ EXAFS signal was extracted using the Athena program and analyzed using the Arthemis program.[16] Fourier transform (FT) of $\chi(k)$ at Zn and Fe *K* edges without phase correction are shown in Fig. 2 and fit results are summarized in Tables I and II, respectively. Similarly to previous works,[9–11] there is a reduction of the amplitude of the main peaks when compared to bulk $ZnFe_2O_4$, associated with the local structural disorder at particle surface layer. Ideally, in normal $ZnFe_2O_4$ the zinc atoms are tetra-coordinated by oxygen at 1.996 Å and 12 Fe atoms are at 3.500 Å as second neighbors. On the other side, iron atoms are surrounded by 6 O at 2.018 Å and 6 Fe atoms at 2.995 Å as second neighbors. We observe that the EXAFS spectra resemble that of the bulk material evidencing that the local structure is almost preserved in nanosized $ZnFe_2O_4$ (Tables I and II). However, an additional peak appears in the FT of the Zn *K*-edge spectrum of 2ZF10h sample (Fig. 2, see arrow). When Zn atoms occupy B sites, a new shell of Fe atoms would appear at $R=2.980$ Å from central Zn. Thus, the similar coordinate *R* obtained from our fit (Table II) indicates that the new peak corresponds to Zn octahedrally coordinated, as reported in Refs. 9–11. The fact that this peak is clearly resolved indicates a large cation transference Zn(A)$\rightarrow$Zn[B] in 2ZF10h. From these EXAFS analysis at both Fe and Zn *K* edges we have determined the degree of inversion, *c*, that represents the site occupancy as $(Zn_{1-c}Fe_c)[Zn_cFe_{2-c}]O_4$, where ( ) and

TABLE II. EXAFS Zn *K*-edge fitted parameters. *c* is the degree of inversion determined according to the Zn *K*-edge EXAFS fitted data.

Sample	Shell	*N*	*R* (Å)	σ^2(Å^2) $\times 10^{-2}$	E_0 (eV)	*c* (%)
2ZF	O[a]	4.6±0.8	2.01±0.02	0.66±0.02	6±1	20
	Fe	13±2	3.51±0.01	1.08±0.02	6±1	
	O	13±2	3.54±0.01	1.08±0.02	6±1	
	Zn	4.4±0.8	3.66±0.01	1.08±0.02	6±1	
2ZF10h	O[a]	4.9±0.8	2.04±0.02	0.9±0.2	3.6±0.8	44
	Fe	0.8±0.4	2.94±0.03	0.3±0.1	−2.6±0.8	
	Fe	11±2	3.49±0.01	1.0±0.2	3.6±0.8	
	O	11±2	3.52±0.01	1.0±0.2	3.6±0.8	
	Zn	3.8±0.8	3.62±0.01	1.0±0.2	3.6±0.8	

[a]A third cumulant was used to fit these shells. Values obtained were $(7\pm2)\times10^{-4}$ and $(8\pm3)\times10^{-4}$ for 2ZF and 2ZF10h, respectively.

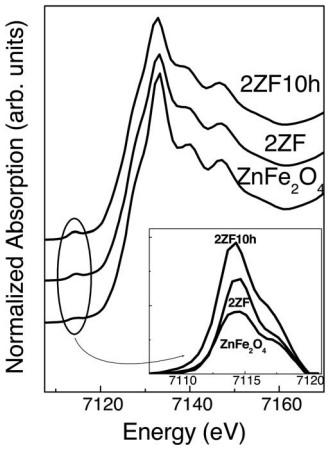

FIG. 3. Experimental XANES spectra at the Fe K edge of 2ZF, 2ZF10h, and bulk $ZnFe_2O_4$. The inset shows the pre-edge region, after discounting the edge jump contribution.

[ ] refer to A and B sites, respectively (Tables I and II). Further, the values obtained from Zn and Fe edges independently are both in good agreement with each other. This discards any site overpopulation in our samples.

All the above results show that milling nanosized $ZnFe_2O_4$ produces an increment of both the grain and magnetic sizes but keeping a nanometric characteristic length, and, at the same time, the inversion increases. We demonstrate that the augment of the degree of inversion in $ZnFe_2O_4$ is not directly associated with a surface effect due to the grain size reduction but with the synthesis process, something that was not clearly stated in previous studies.[2–4,11] In particular, high-energy ball-milling process activates an order-disorder transformation independently whether it is causing an increment or a reduction of the grain/particle sizes.

In the following, we analyze how the near-edge x-ray absorption structure at Fe and Zn K edges are affected by the spinel inversion. Figures 3 and 4 show the Fe-K and Zn-K XANES spectra for nanosized and bulk $ZnFe_2O_4$, respectively. The peak broadening is probably related to cation distribution among locally disordered sites whose energy transition varies according to the average bond length.[17] Fe-K pre-edge structure arises from electronic $1s \rightarrow 3d$ quadrupole and $1s \rightarrow 3d/4p$ (hybridized orbitals) dipole transitions.[18] In agreement with Mössbauer results, the pre-edge position

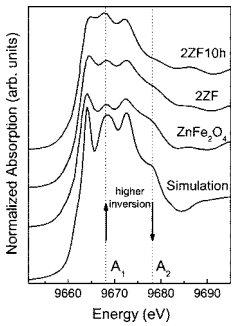

FIG. 4. Experimental XANES spectra at the Zn K edge of nanosized 2ZF and 2ZF10h, bulk $ZnFe_2O_4$, and simulation result of the XANES spectrum of normal $ZnFe_2O_4$ calculated using FEFF8.2.

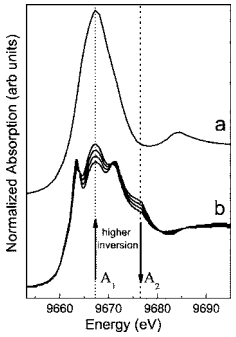

FIG. 5. Theoretical calculation for isolated Zn atom substitutionally replacing Fe at B sites in $ZnFe_2O_4$ structure (a) and theoretical $ZnFe_2O_4$ spectra using weights of 0.0, 0.1, 0.2, and 0.3 for Zn at B sites (b).

is compatible with a Fe^{3+} oxidation state.[19] The integrated intensity of the pre-peaks region progressively increases for 2ZF, 2ZF4h, and 2ZF10h with respect to the bulk compound (see inset in Fig. 3). This is due to the increment of the degree of orbital p-d mixing as more central Fe atoms occupy noncentrosymmetric A sites as follows: 2ZF > 2ZF4h > 2ZF10h. Above the edge, the decrease in amplitude of the white line would also indicate the presence of Fe^{3+} in a four-coordinated surrounding,[17] although, no other remarkable differences were detected in the Fe-K XANES region.

The most striking features due to cation exchange in $ZnFe_2O_4$ appear at the Zn-K edge (Fig. 4), which reflects the electronic transition from zinc $1s$ core level to unoccupied states of p type. Zn-K XANES of normal $ZnFe_2O_4$ consists of three resolved peaks at 9664, 9666.3 (see line A_1 in Figs. 4 and 5) and 9672.4 eV, and a significant shoulder at 9676.7 eV (see line A_2 in Figs. 4 and 5) at the white line region plus additional structure at higher energies (Fig. 4).[20] The spectrum of 2ZF nanoferrite shows some differences at the second feature and the shoulder region (Fig. 4). Furthermore, by increasing inversion the peak positions slightly shift to lower energies, the second feature notably increases in amplitude and the shoulder weakens.

To further study the inversion effects on the Zn-K electronic structure, we have performed XANES simulations using FEFF 8.2 code.[15] Here, we have considered the Hedin-Lundqvist exchange potential with imaginary part of 0.5 eV to simulate experimental broadening.[21] The $Z+1$ approximation (Z, atomic number) for the absorber atom was essential to account for the three main peaks and thus reproduce accurately the experimental data. A 57 atoms cluster (radius of 0.57 nm) was used to calculate the self-consistent field (SCF) muffin-tin atomic potential, and a 185 atoms cluster (radius of 0.805 nm) for the full-multiple scattering (FMS) XANES calculations. For convergence analysis, simulations considering up to 390 atoms (radius of 1.000 nm) and 112 atoms (radius of 0.650 nm) for the FMS and SCF calculations were performed, respectively, and they did not show differences from the results shown here. During the simulation process, the normal spinel $ZnFe_2O_4$ was used as the model structure. The simulated absorption spectrum of the Zn atoms at A sites was obtained using this normal structure.

In the other way, to calculate the spectrum of the Zn absorber at octahedral B-sites, a Zn atom substituted a Fe atom of the model structure, and this Zn atom was used as the absorber during calculations.

Figure 4 shows the theoretical XANES spectrum of normal $ZnFe_2O_4$. The theoretical data was shifted in order to obtain better agreement between the experimental and theoretical $ZnFe_2O_4$ spectra, and all the other theoretical data shown here were shifted by this same value. The very good agreement between experimental and simulated data is evident just by inspection on the main features of the absorption spectra. In addition, the same tendency with the degree of inversion (i.e., transferring Zn atoms from sites with T_d to O_h symmetry) can be observed in simulated set of XANES spectra. Indeed, Fig. 5 shows the theoretical calculation for an isolated Zn atom substituting Fe at an octahedral site in normal $ZnFe_2O_4$ structure [Fig. 5(a)]. It is worth noticing the coincidence between the positions of the second peak of the $ZnFe_2O_4$ structure (line A1) and the white line of the Zn substitutional to Fe in $ZnFe_2O_4$ structure. The substitution of the second and/or fourth coordination shells around the absorber atom, by Zn or Fe atoms, give no significant changes, but causes slight variations in the relative heights of the three main peaks near the edge.

The effect on theoretical XANES spectra of increasing Zn population at B sites in $ZnFe_2O_4$ [Fig. 5(b)] was calculated by the weighted sum of both normal spinel spectrum (Zn occupying A sites, shown in Fig. 4) and the spectrum of a Zn absorber substitutional to Fe atom at B sites [Fig. 5(a)]. The four spectra in Fig. 5(b) were obtained using weights of 0.0, 0.1, 0.2, and 0.3 for the Zn at B sites (the degree of inversion), and consequently weights of 1.0, 0.9, 0.8, and 0.7 for Zn at equilibrium A sites. Arrows in Fig. 5 indicate the tendency of each feature with increasing inversion. The results show not only the intensity enhancement at 9666.3 eV (see line A_1 in Figs. 4 and 5) but also the amplitude reduction of the shoulder near 9676.7 eV (see line A_2 in Figs. 4 and 5), with increasing concentration of Zn at the otherwise Fe equilibrium location in $ZnFe_2O_4$. Both trends coincide with those observed experimentally, showing the important local structural changes in nanostructured zinc ferrite that involve a considerable zinc cation transference from A to B sites that modifies its electronic structure. It is worth mentioning that when we consider a weight of 0.5 for the Zn in octahedral B sites the main features of the XANES disappears and the white line dominates the spectrum shape.

Summarizing, chemically prepared $ZnFe_2O_4$ nanocrystalline displays an inverted structure that changes its long-range magnetic order and enhances its magnetic response with respect to bulk antiferromagnetic material. This is in accordance with all previous results on nanosized $ZnFe_2O_4$ independent on the synthesis procedure. We demonstrate that the mechanical crystallization that takes place on nanocrystalline spinel, which involves both grain and apparent magnetic size growth, is also accompanied by a significant augment of the inversion. This result shows that the inversion involves the whole particle and is not only restricted to a more distorted surface layer.

On the other hand, XANES results give a direct proof of the nonequilibrium cation distribution through the Fe *K*-edge pre-edge features but mainly through Zn *K*-edge features, which change due to the particular configuration of the ligand shells surrounding the absorbing atom. These features are intensified by the cationic swap originated by transferences of type $Zn^{2+}(A) \rightarrow Zn^{2+}[B]$ and $Fe^{3+}[B] \rightarrow Fe^{3+}(A)$ that take place preserving the structural long-range order of the compound. Thus, superexchange interactions $Fe^{3+}[B]—O^{-2}—Fe^{3+}(A)$ emerge and confer $ZnFe_2O_4$ a cluster glass or ferrimagnetic magnetic behavior.[3] The large zinc occupancy of octahedral sites that we found cause broken superexchange A-B paths by the presence of nonmagnetic ions (Zn^{2+}) that, in addition to an inhomogeneously distributed inversion, bring about regions where ferrimagnetic A-B or antiferromagnetic B-B interactions coexist.[5] On the other hand, considering that the magnetic properties of ferrimagnetic material are critically dependent on site occupancy, XANES approach as outlined here promises to be an important tool in determining the structure of these materials. Further, our results encourage future effort to understand the electronic structure throughout the unusual Zn *K*-edge near-edge features of $ZnFe_2O_4$ (Ref. 20) or investigate suggested electron density anomalies in nanosized $ZnFe_2O_4$ (Ref. 22).

We appreciate financial support by LNLS synchrotron, Campinas—SP, Brazil (Project No. D04B-XAFS1 # 4148/05); ANPCyT, Argentina (PICT03 06-17492); CONICET, Argentina (PIP 6524 and PIP 6075). DC magnetic measurements were performed using the RN3M facilities. We thank E.D. Cabanillas for TEM microscope operation and F. Sives for fruitful discussions.

*Corresponding author. E-mail address: stewart@fisica.unlp.edu.ar

[1] H. H. Hamdeh *et al.*, J. Appl. Phys. **81**, 1851 (1997).
[2] C. N. Chinnasamy *et al.*, J. Phys.: Condens. Matter **12**, 1 (2000).
[3] M. Hofmann *et al.*, J. Mater. Sci. **39**, 5057 (2004).
[4] M. K. Roy *et al.*, Nanotechnology **17**, 232 (2006).
[5] J. H. Shim *et al.*, Phys. Rev. B **73**, 064404 (2006).
[6] F. S. Li *et al.*, J. Magn. Magn. Mater. **268**, 332 (2004).
[7] S. A. Oliver *et al.*, Phys. Rev. B **60**, 3400 (1999).
[8] E. J. Choi *et al.*, J. Magn. Magn. Mater. **301**, 171 (2006).
[9] B. Jeyadevan *et al.*, J. Appl. Phys. **76**, 6325 (1994).
[10] S. A. Oliver *et al.*, Appl. Phys. Lett. **76**, 2761 (2000).
[11] S. Ammar *et al.*, J. Non-Cryst. Solids **345**, 658 (2004).
[12] S. J. Stewart *et al.*, Physica B **389**, 155 (2007).
[13] A. Kundu *et al.*, Phys. Lett. A **311**, 410 (2003).
[14] R. D. K. Misra *et al.*, Mat. Scie. Lett. B **111**, 164 (2004).
[15] J. J. Rehr *et al.*, Phys. Rev. B **34**, 4350 (1986).
[16] B. Ravel *et al.*, J. Synchrotron Radiat. **12**, 537 (2005).
[17] G. A. Waychunas *et al.*, Phys. Chem. Miner. **10**, 1 (1983).
[18] F. de Groot, Chem. Rev. (Washington, D.C.) **101**, 1779 (2001).
[19] M. Wilke *et al.*, Am. Mineral. **86**, 714 (2001).
[20] G. A. Waychunas *et al.*, Geochim. Cosmochim. Acta **67**, 1031 (2003).
[21] M. Roy and S. J. Gurman, J. Synchrotron Radiat. **8**, 1095 (2001).
[22] C. Upadhyay *et al.*, Appl. Phys. Lett. **85**, 2074 (2004).